
ENERGY COUPLING IN LINED HOHLRAUMS (HLP1, HLP2, AND HLP7)

<i>R. L. Kauffman</i>	<i>C. W. Hatcher</i>	<i>D. W. Phillion</i>	<i>R. J. Wallace</i>
<i>L. J. Suter</i>	<i>H. N. Kornblum</i>	<i>J. L. Porter*</i>	<i>P. E. Young</i>
<i>R. L. Berger</i>	<i>E. F. Lindsey</i>	<i>M. D. Rosen</i>	<i>F. Ze</i>
<i>C. B. Darrow</i>	<i>D. S. Montgomery</i>	<i>R. Thiessen</i>	<i>J. C. Fernandez**</i>
<i>S. N. Dixit</i>	<i>T. E. Orzechowski</i>	<i>R. E. Turner</i>	<i>J. A. Cobble**</i>

Introduction

Indirect-drive inertial confinement fusion (ICF) uses high- Z cavities, or hohlraums, to confine x rays for compressing and igniting deuterium-tritium fuel contained in spherical capsules.^{1,2} For laser-driven ICF, the intense laser beams enter the hohlraum through small laser entrance holes (LEHs), heating the high- Z hohlraum walls. The laser-produced radiation heats the unirradiated high- Z walls producing a nearly isotropic radiation environment for spherically compressing the ICF capsule.² The radiation flux on the capsule is not completely isotropic, however, because the laser-irradiated area is generally brighter than the surrounding x-ray heated walls and the LEHs do not radiate. Furthermore, the angular distribution of flux on the capsule is time dependent because the unilluminated walls become hotter and more emissive as a function of time, and plasma dynamics cause the laser-irradiated area to move. Symmetric implosions are obtained by dynamically balancing the effects of the LEHs, wall heating, and laser-spot motion.³

The laser absorption and thus radiation symmetry depend on the dynamics of the hohlraum plasma. For long pulses, such as those required for ignition targets on the proposed National Ignition Facility (NIF), a large volume of the hohlraum can fill to plasma electron densities of $n_e \approx 10^{21} \text{ cm}^{-3}$ or greater, which can cause significant movement of the absorption region. In NIF hohlraum designs, a low- Z plasma replaces the low-density, high- Z blowoff to better control the laser-spot motion.

Inverse bremsstrahlung is lower in the low- Z plasma compared with a high- Z plasma at the same density, allowing the laser to deposit its energy in higher-density, high- Z plasma nearer the initial wall position.^{2,4} Calculations indicate that the low- Z plasma reduces

the movement of the laser deposition region, making symmetry more easily obtainable. For initial NIF target designs, the low- Z underdense plasma was produced by initially coating the high- Z wall with low- Z material. The laser and radiation ablate the thin low- Z coating from the wall, filling the hohlraum with low- Z plasma. For more recent designs, the hohlraum is initially filled with low- Z gas which, when ionized, produces the underdense low- Z plasma. Gas-filled hohlraums avoid problems with plasma stagnation and jetting, which computationally degrade capsule symmetry in the lined-hohlraum designs.

NIF designs using low- Z plasma to control spot motion had not previously been tested. Many of the Hohlraum and Laser Physics (HLP) tasks for the Nova Technical Contract (NTC) were developed to experimentally test the physics for low- Z lined hohlraums. Specifically, HLP1 and HLP2 are tasks to test the energetics of lined hohlraums and to understand the scaling to NIF hohlraums within the energy and power constraints of Nova. HLP1 experiments investigate drive using shaped pulses where the underdense plasma evolution better approximates the NIF plasma but at lower powers than attainable on the NIF. The goal of HLP1 is to demonstrate acceptable laser coupling in hohlraums with a shaped drive pulse producing radiation temperatures T_R in the range of ~ 100 to ~ 210 eV. HLP2 experiments investigate drive in lined hohlraums at high powers to understand radiation drive scaling to NIF peak drive regimes. HLP2 goals are to demonstrate acceptable coupling in hohlraums with T_R of ≥ 270 eV. For both tasks, acceptable coupling is defined as absorption fraction $f_{\text{abs}} > 90\%$; stimulated Brillouin scattering (SBS) fraction $f_{\text{SBS}} < 5\text{--}10\%$; hot electron fraction $f_{\text{hot}} < 5\%$ at a hot electron temperature, $T_{\text{hot}} \geq 50$ keV, and stimulated Raman scattering (SRS) fraction $f_{\text{SRS}} < 5\%$.

* Sandia National Laboratories, Albuquerque, New Mexico

** Los Alamos National Laboratory, Los Alamos, New Mexico

Results from both HLP1 and HLP2 experiments successfully attain the drive goals defined in the NTC, although the liner does reduce the peak drive compared with experiments using unlined hohlraums. Calculations partly predict this reduction in drive as being due to enhanced hydrodynamic losses to the underdense plasma. Although the diagnostics were not optimal, measurements of SBS using subaperture sampling and SRS using x-ray bremsstrahlung from fast-electron production suggest that enhanced plasma instability production in the lined hohlraums also contributes to the observed reduced drive. The drive experiments performed for HLP1 and HLP2 use unsmoothed laser beams. Recent experiments demonstrate that stimulated scattering levels are reduced to about the 1% level using beam-smoothing techniques. These experiments are described in “Laser-Plasma Interactions in NIF-Scale Plasmas (HLP5 and HLP6)” on p. 305 of this *Quarterly*. For the same laser intensity and pulse length, x-ray conversion efficiency inferred in hohlraums is significantly higher than that obtained from isolated flat foils. The HLP task is focused on experiments to understand this difference.

Experiments

Experiments on Nova use hohlraums whose shape is a right circular cylinder, shown schematically in Fig. 1(a). Nova scale-1 hohlraums are Au and are 1.6 mm diam \times 2.55–2.75 mm long. Typically, the hohlraum wall thickness is 25 μm , and in some experiments is thinned to $\sim 2 \mu\text{m}$ to image kilo-electron-volt x rays through the wall. Different hohlraum lengths are sometimes used for symmetry or for satisfying other experimental constraints. Different hohlraum sizes are scaled from the scale-1 size by the ratio of their dimensions to those of a scale-1 size. For example, a 0.75-scale hohlraum is 1.2 mm diam \times 2 mm long. The LEH is varied, depending on the experiment, from 50 to 100% of the hohlraum diameter. For the energetics scaling, the results are scaled to 50% LEH for the square pulses and 75% for the shaped pulses, unless otherwise noted. For all of the energetics studies, the hohlraums are empty, not containing a fuel capsule.

The lined hohlraums are coated with either Ni or CH in the form of parylene. The parylene coating is done using vacuum deposition and by allowing the parylene to enter through the LEHs and randomly collide with the wall until it sticks. Since parylene has a low probability of sticking when colliding with a solid surface, it statistically has many collisions with the wall before it sticks. This method can produce uniform surfaces even on the inside hohlraum wall. Typically, the coating thickness is 0.75 μm with a density $\rho \approx 1.10 \text{ g/cm}^3$ unless otherwise stated. When fully ionized, this layer would fill the initial volume to a density of $\sim 10^{21}$ electrons/ cm^3 . The coating thickness is characterized by measuring

the Au x-ray fluorescence from a scanning electron microscope (SEM). The SEM signal is calibrated using a series of flat Au targets overcoated with various thicknesses of parylene. The coating thicknesses on the flat targets are characterized using optical interferometry and a stylus profilometer. In this way, coating thickness for the hohlraums can be measured to an accuracy of $\pm 20\%$. Uniformity along the inside hohlraum wall is checked using the SEM by cutting open test hohlraums. Also, coating thicknesses on a target used for an experiment could be checked by measuring the thickness on the outside wall.

Ni-coated hohlraums are made using electrodeless Ni plating. The coating is 88% Ni by weight with the remaining 12% by weight being P. Its average density is 8.2 g/cm^3 , with the nominal coating thickness of 0.15 μm . Thicknesses on hohlraums are also character-

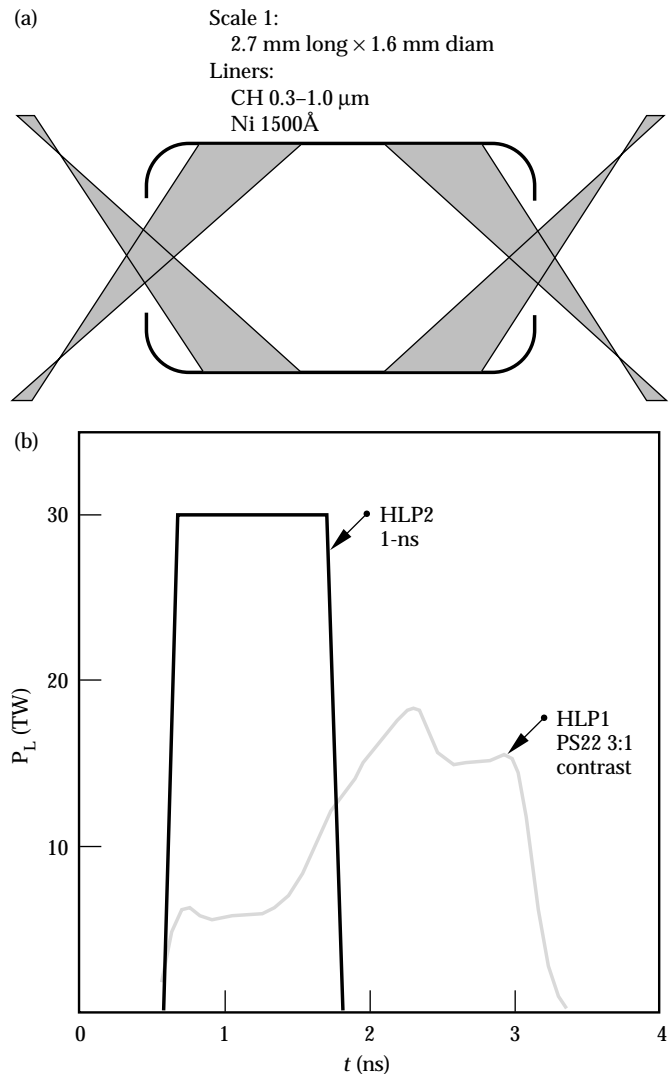


FIGURE 1. Schematic of hohlraum drive experiments. (a) The hohlraum and irradiation geometry. (b) Representative pulse shapes of the incident laser pulses at 0.35 μm wavelength. PS22 is a 3:1 contrast shaped pulse for HLP1 and HLP2, using a 1-ns square pulse with a maximum power of 30 TW. (20-05-0995-2111pb01)

ized using the SEM, measuring the relative x-ray fluorescence signal of Ni compared with Au. Again, the system is calibrated using coated Au flats. Errors in thickness are estimated to be $\pm 20\%$.

Hohlraums are irradiated using the 10 Nova laser beams, 5 per side. Figure 1(b) shows the laser pulses. The pulse shape for HLP1, designated PS22, is a 2.2-ns-long pulse with a 3:1 contrast between the peak intensity and the foot intensity. This is the same pulse shape used for the bulk of the pulse-shaped symmetry experiments described in the next article, “Nova Symmetry: Experiments, Modeling, and Interpretation (HLP3 and HLP4),” on p. 293. Pulse shapes for HLP2 are 1-ns-long approximately square pulses with total powers up to 30 TW (maximum power available on Nova). The beams are pointed through the center of the LEH and defocused to reduce the intensity of the laser on the wall, shown schematically in Fig. 1(a). For a scale-1 target, the defocusing is ~ 1 mm, in the diverging direction from best focus, at the LEH. This allows ~ 100 μm clearance of the beam for a 50% LEH, assuming geometrical optics for an $f/4$ beam. The beam irradiates the wall of the hohlraum at an angle of 40° with respect to the normal of the wall and has a first bounce intensity of $\sim 8 \times 10^{14}$ W/cm^2 for 2 TW of laser power P_L per beam.

Diagnosics

X-ray drive is measured using two complementary techniques.⁵ One technique measures the shock wave generated by the absorbed x-ray flux in an Al witness plate. The Al witness plate is a piece of Al whose thickness continuously varies from one end to the other, or has discrete steps of known thickness, placed over a hole in the hohlraum wall. The shock front is measured by observing the optical emission produced by the emerging shock at the rear of the Al plate. The optical emission is measured using an ultraviolet (UV) Cassegrain telescope coupled to an optical streak camera. X-ray drive is derived by comparing the measured shock velocity with hydrodynamic calculations or semi-empirical models as described in the article “Planar and Cylindrical Rayleigh–Taylor Experiments on Nova (HEP2),” p. 232. The estimated error for measuring drive is ± 5 eV, which includes the accuracy of the measurement and the uncertainty in the comparison with the calculations. The other technique measures the x-ray flux irradiated from the hohlraum wall using an array of x-ray diodes (XRD).⁶ A number of broadband channels are defined in the range from 0.1 to 1.8 keV using thin absorption filters and, for some channels, grazing incident x-ray mirrors. The XRD array measures the hohlraum drive by measuring the flux from an opposite wall in the hohlraum through a hole in the hohlraum wall. The hole is lined with Be to prevent high- Z plasma from occluding the line of sight into the hohlraum. Time-resolved spectra are unfolded from

the signals using calibrated channel response. The time resolution is on the order of 150 ps limited by the bandwidth of the detectors and oscilloscopes and the correlation of the timing among the detectors. The spectrally integrated flux is measured to an accuracy of $\sim 20\%$ including calibration accuracies and unfolding uncertainties resulting in a $\pm 5\%$ uncertainty when converted to an equivalent radiation drive temperature.

The two measurement techniques are complementary since the shock velocity measures the flux incident on the wall while the XRD array measures the reradiated flux. The two are related by the wall albedo,² or effective reflectivity. The shock velocity is best suited for measuring peak drive and can provide only coarse time-dependent measurements. The XRD array provides much better time-dependent reradiated flux measurements, but the data must be corrected for albedo, which is time dependent, to obtain incident x-ray flux. For both techniques, the measurement is usually made in the midplane of the hohlraum between the two sets of beam cones where it is not directly irradiated by the laser. The flux on the ICF capsule, or other areas of the hohlraum, must be derived using detailed radiation hydrodynamic calculations or semi-empirical view factor estimates.

Laser coupling is also studied by measuring the scattered light and x-ray bremsstrahlung produced by superthermal electrons. SBS light into the lens is measured using a subaperture sampling on one of Nova’s ten beamlines, beamline six (BL6).⁷ The light from approximately 5% of the beam area is extracted from the reflected beam using an uncoated piece of fused silica. It is then optically relayed to a diagnostic table equipped with an optical calorimeter, a fast-photodiode coupled to a Tektronix 7912 transient digitizer, and a time-resolved optical spectrometer. The calorimeter and photodiode are absolutely calibrated by placing a partially reflecting retroreflector in front of the calorimeter mounted opposite BL6. The retroreflector reflects 7.6% of the incident energy, and the data is reduced assuming the incident light and backscattered light uniformly fill the lens aperture. More recent experiments with improved diagnostics developed for HLP5 [as discussed in “Laser–Plasma Interactions in NIF-Scale Plasmas (HLP5 and HLP6)” on p. 305] have shown that there can be significant variations in the near-field distribution of the backscattered light in the lens aperture as well as some light being scattered outside of the lens.⁸ The scattered light data presented here have large uncertainties due to the subaperture sampling, but the relative trends in the data among different target types should be qualitatively valid.

Fast-electron production from SRS is studied by measuring the x-ray bremsstrahlung from the target in the 20–200-keV spectral range.⁹ The x rays are produced when the fast electrons deposit their energy in the high- Z case. For most of the measurements,

hohlraums with thin walls ($\sim 2\text{--}3\ \mu\text{m}$) are used to minimize x-ray absorption in the hohlraum walls. This measurement does not include fast electrons that escape the target or that lose their energy in the plasma before reaching the wall. In addition, time-resolved SRS light spectra are measured 28° from an incident beamline. Also, a photodiode array measures the angular distribution of the SRS light. SRS light was not measured inside of the lens cone. Recent experiments have shown that a significant amount of SRS light can be scattered into the lens cone.⁸

Results

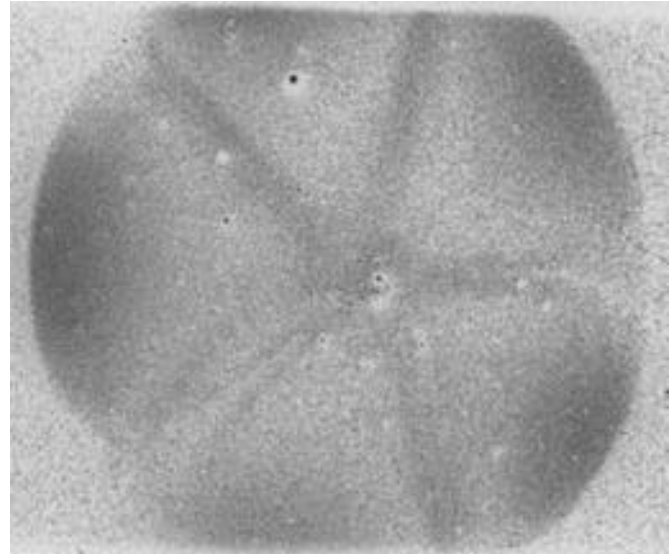
Lined hohlraums reduce the amount of high- Z material filling the interior of the hohlraum. The effect of liners on plasma filling can be seen qualitatively in Fig. 2, which shows time-resolved images of kilovolt x rays viewing along the axis of Nova hohlraums.¹⁰ Figure 2(a) is an image of an unlined hohlraum, and Fig. 2(b) shows a hohlraum lined with $0.75\ \mu\text{m}$ of CH. Both images are taken at around $1.5\ \text{ns}$ after the beginning of PS22, which is near the peak of the laser intensity. Both images show five bright spots placed nearly equally inside of the hohlraum. These spots are Au blowoff from the laser beams irradiating the hohlraum walls. The hohlraum wall itself is masked by the LEH, which defines the viewing area. For the unlined hohlraum, the figure also shows five spokes and a central bright spot. These are produced by stagnation of the high- Z plasma from the wall blowoff, indicating that by this time the high- Z plasma has filled the laser irradiation part of the hohlraum. For the lined hohlraum, the bright spokes and central region are replaced by an absence of emission. This region is filled by low- Z CH plasma, which is a much poorer radiator than high- Z plasma. These images indicate that qualitatively, at least, low- Z plasma does reduce the filling of the hohlraum by high- Z plasma.

Drive at high power has been investigated using 1-ns square pulses for HLP2. Figure 3 shows peak T_R measured using shock breakout for both CH- and Ni-lined hohlraums. Data are included for both scale-1 and scale-0.75 hohlraums. Most of the data are taken with 2.55-mm -long hohlraums. Some of the data are from longer hohlraums and have been corrected ($<5\ \text{eV}$) to account for this. The data is plotted as a function of $P_L/\text{wall area}$ where the wall area is the total area of the hohlraum not corrected for LEH or diagnostic holes. Drive from unlined hohlraums, reported previously, is also plotted for comparison.¹¹ Drive from lined hohlraums is below the measured drive for unlined hohlraums. Table 1 summarizes the average reduction in drive for lined hohlraums compared with unlined hohlraums. The uncertainties listed in Table 1 are the

standard deviations of the data set. For scale-1 targets, the reduction is $16\text{--}18\ \text{eV}$, representing $\sim 25\text{--}30\%$ decrease in available x-ray drive for both CH- and Ni-lined hohlraums.

Figure 4 shows drive from lined hohlraums heated with shaped pulses. Figure 4(a) shows the time-resolved drive derived from the XRD array for both CH- and Ni-lined hohlraums compared with drive measured from

(a) Unlined hohlraum



(b) Lined hohlraum

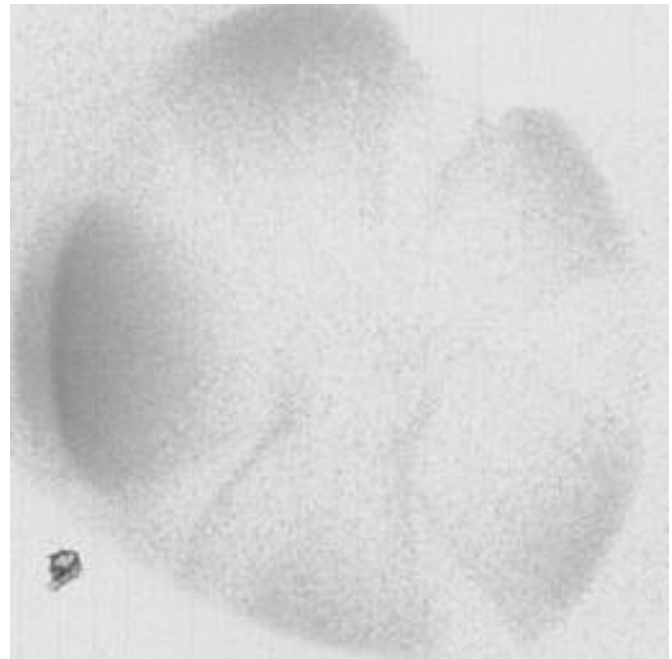


FIGURE 2. X-ray images of the hohlraum heated with PS22 viewing along the axis of the cylinder. The time-resolved images are taken at approximately $1.5\ \text{ns}$, which is about the peak of the laser pulse. The image in (a) is from an unlined hohlraum and (b) is from a hohlraum lined with $0.75\ \mu\text{m}$ CH. (20-05-0995-2112pb01)

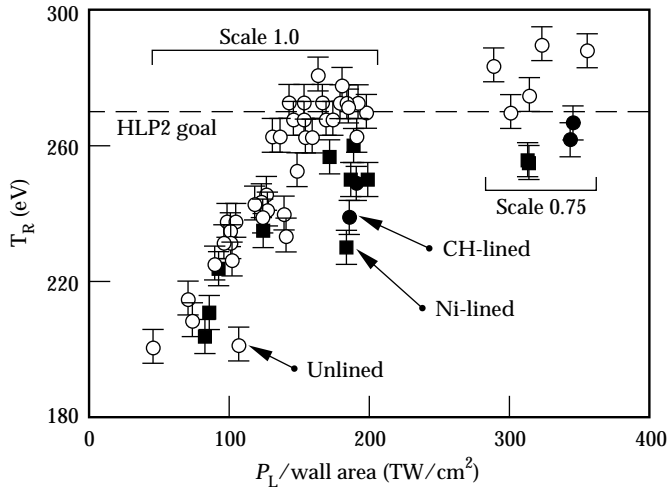


FIGURE 3. Peak radiation temperature T_R measured in scale-1 and scale-0.75 hohlraums heated with 1-ns square pulses of 0.35- μm light. Measurements are made using the shock breakout technique in Al witness plates. Open circles are from unlined Au hohlraums and closed circles and closed squares are from CH- and Ni-lined hohlraums, respectively. The HLP2 goal of 270 eV is shown as a dashed line. (20-05-1093-3696pb01)

TABLE 1. Reduction in drive of lined hohlraums compared with unlined hohlraums.

Hohlraums	ΔT_R (eV) experiment	ΔT_R (eV) LASNEX
Scale 0.75		
1 ns, 1500 \AA Ni, 25 TW	26 ± 9	—
1 ns, 7500 \AA CH, 25 TW	17 ± 9	—
Scale 1.0		
1 ns, 1500 \AA Ni, 12 TW	16 ± 3	14
1 ns, 1500 \AA Ni, 25 TW	18 ± 6	14
PS22, 1500 \AA Ni	18 ± 5	14
PS22, 4000 \AA CH	6 ± 3	9
PS22, 7500 \AA CH	11 ± 9	12

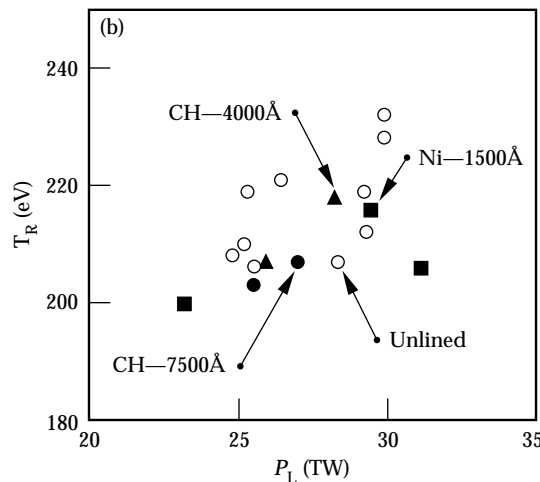
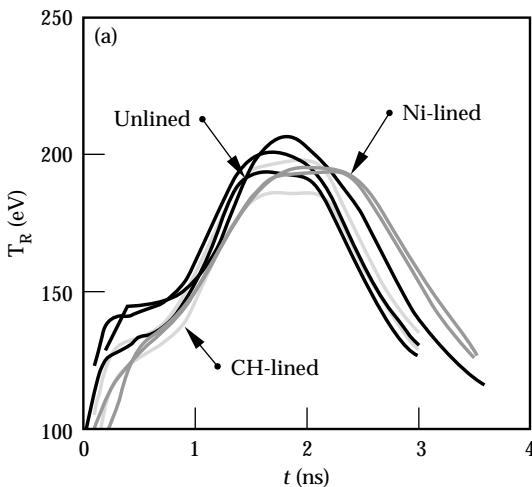


FIGURE 4. Radiation drive measured from scale-1 hohlraums heated with 0.35- μm light using PS22. (a) Compares time-resolved Dante measurements of the drive from unlined and CH- and Ni-lined hohlraums. (b) Shows peak drive measured using the shock breakout technique in Al witness plates from the different targets. (20-05-1093-3696pb01)

unlined hohlraums. The main differences in the drive between the lined and unlined hohlraums are that the beginning of the drive is delayed in the initial foot of the pulse and that the peak drive is less for lined hohlraums. Figure 4(b) plots the peak drive as measured from the shock breakout, which also confirms the reduction in peak drive for lined hohlraums. The difference in peak drives for Figs. 4(a) and (b) is the correction for wall albedo. The delay in the beginning of the drive can be understood qualitatively as the reduction in x-ray flux initially as the laser burns through the liner before heating the Au walls. As summarized in Table 1, the reduction in peak drive for lined hohlraums is ~ 20 – 30% of the x-ray flux for unlined hohlraums. Drive data from unlined hohlraums have been empirically fit with a simple power balance model.¹¹ This simple model balances the heating sources with the heat losses. The heating source is the x-ray energy produced by the incident laser drive heating the hohlraum walls. The heat losses are the energy absorbed by the hohlraum walls and energy radiated through the laser entrance and diagnostic holes.^{12,13} The hohlraum wall loss is modeled using a Marshak scaling¹⁴ for wall loss. The power balance equation is

$$\eta_{\text{HOHL}} P_L = \sigma T_R^4 A [1 - \alpha(1 - f_H)]. \quad (1)$$

The source term on the left is the incident P_L multiplied by the effective efficiency for converting laser light to drive energy, η_{HOHL} . The loss terms are on the right. σ is the Stefan-Boltzman constant, A is the hohlraum area, f_H is the fraction of the hohlraum area that is holes, and α is the wall albedo. All of the parameters in the equation can be determined independently by the experimental geometry and the measurement except for η_{HOHL} and α . α is both time and temperature dependent. It can be calculated from LASNEX or simple

models of radiation wave scaling and depends on the opacity and equation of state for the material.

Figure 5 shows the data fit with Eq. (1) from the scale-1 hohlraums heated with square pulses. The fits use power-law scaling of α derived from self-similar solutions to Marshak's wave heating of materials with power-law dependencies for opacity and equation of state.^{12,13} η_{HOHL} is treated as a fitting parameter. Results of the fits are shown Fig. 5. For unlined hohlraums, $\eta_{\text{HOHL}} \approx \sim 0.75$ while $\eta_{\text{HOHL}} \approx 0.53$ to 0.64 for the lined hohlraum data. This simple model suggests that the effective coupling is reduced by 15–30%. The data set is much sparser for the scale-0.75 data, but it is consistent with similar reduction in effective coupling. The pulse-shaped data cannot be fit easily with an analytic model because of the dependence of α on time and temperature, but the decrease in drive is approximately similar to the 1-ns square results, and therefore the reduction in coupling is expected to be similar.

The reduced coupling for lined hohlraums can be due to several effects. Some reduction is expected, as discussed in the next section, because of the energy expended to heating the liner and to differences in coupling to hydrodynamic motion. Other potential differences are decreased absorption due to higher levels of reflected light, SBS, and SRS.

The absorption is studied by measuring both the scattered SBS and SRS light and fast electrons produced by SRS. Table 2 shows the fraction of SBS light scattered into the lens for the various targets for both CH- and Ni-lined hohlraums. The data are taken using the subaperture sampling, as discussed earlier. The quoted errors are the standard deviations of the data scatter and are not intended to represent the total error in the experiment. The CH- and Ni-lined hohlraum experiments were done at different periods on the laser, and the unlined data acquired during the two periods are listed separately for meaningful comparison. The two sets of unlined data show that the measurements are reproducible.

Within the data scatter, no increase in SBS from CH-lined hohlraums is observed compared with SBS from unlined hohlraums. For Ni-lined hohlraums, higher SBS levels are observed for both scale-0.75 hohlraums heated with 1-ns square pulses and scale-1 hohlraums heated with PS22. The scale-0.75 hohlraum data during the Ni-lined experiments consist of only two data points for the Ni-lined hohlraums and one data point for the unlined hohlraums. This increase is therefore based on a sparse data set, but it is apparently real. For the CH-lined scale-0.75 data set, there are three data points for the unlined hohlraums and five data points for the CH-lined hohlraums. There are many shots for the PS22 data, and the increase in scattering for the Ni-lined hohlraums is apparently real. Some of the large scatter in the data may be due to changes in experi-

mental conditions such as changes in the focusing. Some of the data were taken during symmetry studies where the crossing point of the beams changed with respect to the LEH. Some correlations in the data could be observed with the change in focusing.³ When scattering data from unlined and Ni-lined hohlraums are compared with similar targeting geometries, scattering levels from Ni-lined hohlraums are consistently higher, although quantitative levels differ.

A significant limitation to these measurements is due to the subaperture sampling and the assumption that it represents the average over the entire beam cone. A full-aperture backscattering station (FABS) as well as a near backscatter imaging (NBI) system have been implemented on Nova since these experiments were done.⁸ These diagnostics can make near-field measurements of the SBS up to angles of 14° from direct backscatter around beamline 7 (BL7). They have shown that SBS from hohlraums is well collimated but can be shifted with respect to direct backscatter for some targets.¹⁵ Although no experiments have been done with lined targets since the FABS and NBI have been fielded, results from the FABS and NBI can be

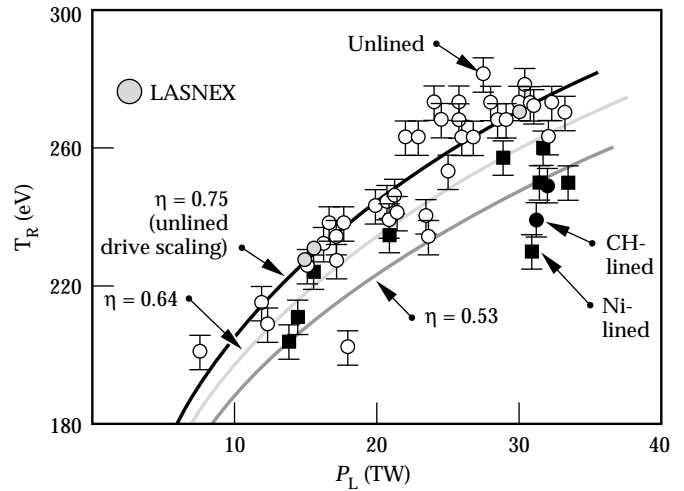


FIGURE 5. Drive scaling for scale-1 hohlraums heated with 1-ns pulses. The data is the same as presented in Fig. 1. The curved lines are fits to the power balance model with different coupling efficiencies. Results of 2-D LASNEX modeling for unlined hohlraums are also shown. (20-05-1093-3697pb01)

TABLE 2. SBS reflectivity from lined hohlraums.

	CH data		Ni data	
	Unlined	CH-lined	Unlined	Ni-lined
1 ns scale 1	$1.5 \pm 1\%$	$2.8 \pm 0.6\%$	$1.6 \pm 1\%$	$1.7 \pm 1.2\%$
1 ns scale 0.75	$4.6 \pm 1.3\%$	$4.5 \pm 1.6\%$	3.5*	$8.7 \pm 0.3\%$
PS22 scale 1	$5.8 \pm 2.9\%$	$4.5 \pm 2.9\%$	$7.3 \pm 4.7\%$	$15.1 \pm 5.3\%$

*Value represents only one experiment.

compared with the subaperture results for unlined hohlraums. In all cases, the SBS into the lens measured by FABS alone is about half of the results listed in Table 2 for unlined hohlraums. Generally, SBS levels measured with NBI are comparable to those measured by FABS so that the total SBS from unlined hohlraums is comparable to the levels listed in Table 2. This may be purely coincidental, and there is no guarantee that it applies to the lined hohlraum results.

Time-resolved SBS spectra are measured using a grating spectrometer coupled to an optical streak camera. Figure 6 shows an example of the data, displaying isointensity contours of the two-dimensional (2-D) image. The spectral and time resolution are of 3 Å and 30-ps, respectively. Spectra from Ni-lined hohlraums for both 1-ns square and PS22 pulses are red-shifted by 7–8 Å relative to the incident light wavelength.

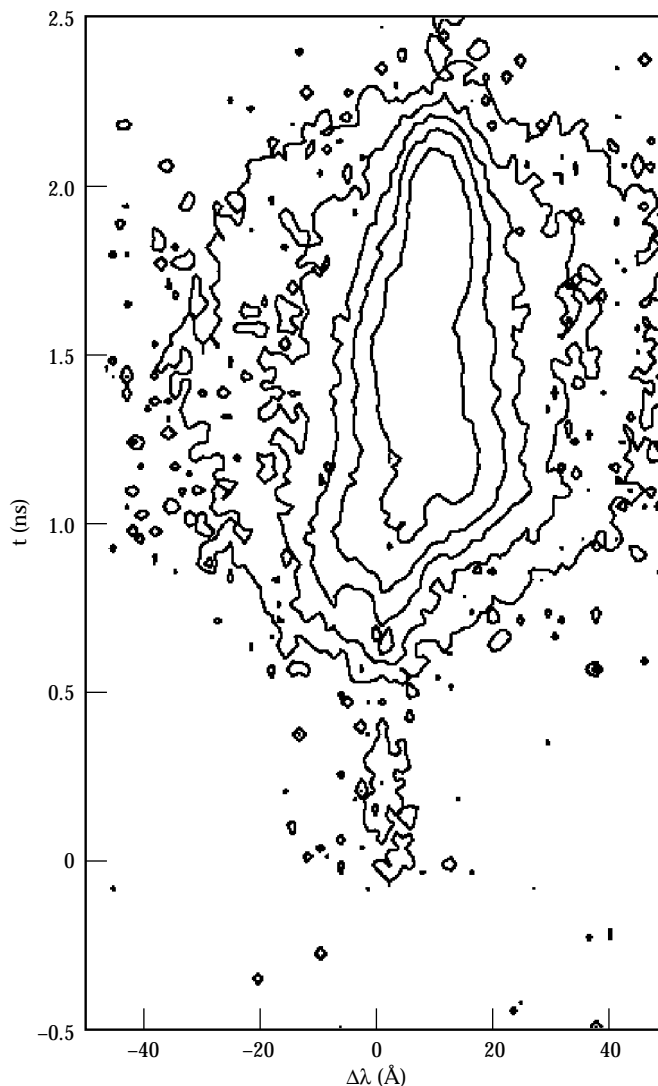


FIGURE 6. Spectrum vs time contour plot of SBS light from a Ni-lined hohlraum. The spectral shift is measured from the incident 0.35- μm wavelength light. (20-05-1095-2364pb01)

Typically, the spectra from unlined hohlraums show little or no shift. This is qualitatively similar to disk targets where the SBS spectrum is shifted more to the blue for high-Z targets compared with low-Z targets. SBS spectra from hohlraums are more red shifted than SBS spectra from disks at similar irradiances. This is presumably due to less Doppler shift, because the plasma flow in the backscatter direction is reduced by the hohlraum, confining the plasma.

As shown in Fig. 7, the spectral data can be integrated over wavelength to obtain the time history of SBS. The time history has been normalized to the calorimeter data for this shot to obtain time-resolved reflectivity. Figure 7 also shows the incident laser pulse. For PS22, the intense part of the SBS signal begins around 1.3 ns, when the incident laser pulse power begins to increase and lasts during the entire high-intensity part of the pulse. A small signal is seen at the beginning of the pulse, but it is a factor of 100 lower. Time history of SBS from 1-ns pulses heating scale-1 hohlraums are qualitatively similar. A signal is seen during the first 300 ps and then it goes away. A second feature turns on at around 700 ps, lasting the rest of the pulse. The intensity of the initial feature is higher because the incident beam intensity is higher for 1-ns pulses compared with PS22.

Fast-electron production is studied by measuring the x-ray bremsstrahlung from electrons depositing their energy in the hohlraum walls. Figure 8 shows spectra from experiments using both PS22 and 1-ns pulses. For PS22, the superthermal electron production is quite low. Using the expression derived from thick target bremsstrahlung for converting x rays to electron flux,¹⁶ the superthermal electron levels for PS22 are less than 0.1% for all of the targets. For comparison, the

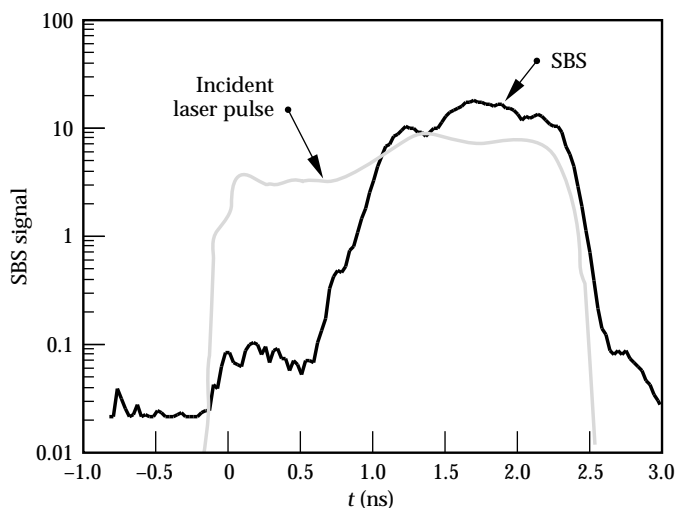


FIGURE 7. Time history of the backscattered light into the BL6 lens. The time history is derived from integrating in wavelength the time-resolved spectrum shown in Fig. 6 and normalizing the time history to the total backscattered light. (20-05-1095-2366pb01)

black line in Fig. 8 is the x-ray spectrum calculated assuming 1% of the incident laser energy is converted to a 50 keV superthermal electron tail. The calculated spectrum does not include self absorption in the target. The data for both lined and unlined hohlraums are an order of magnitude lower. The hot-electron temperatures for the Ni-lined and unlined hohlraums are ~ 50 keV while the CH-lined hohlraums have slightly lower hot-electron temperatures (~ 40 keV). A limited amount of data was taken measuring the SRS light levels using diodes positioned around the chamber. The integrated SRS is ~ 0.2 – 0.4% , which is slightly higher than levels that would be inferred from fast-electron levels.

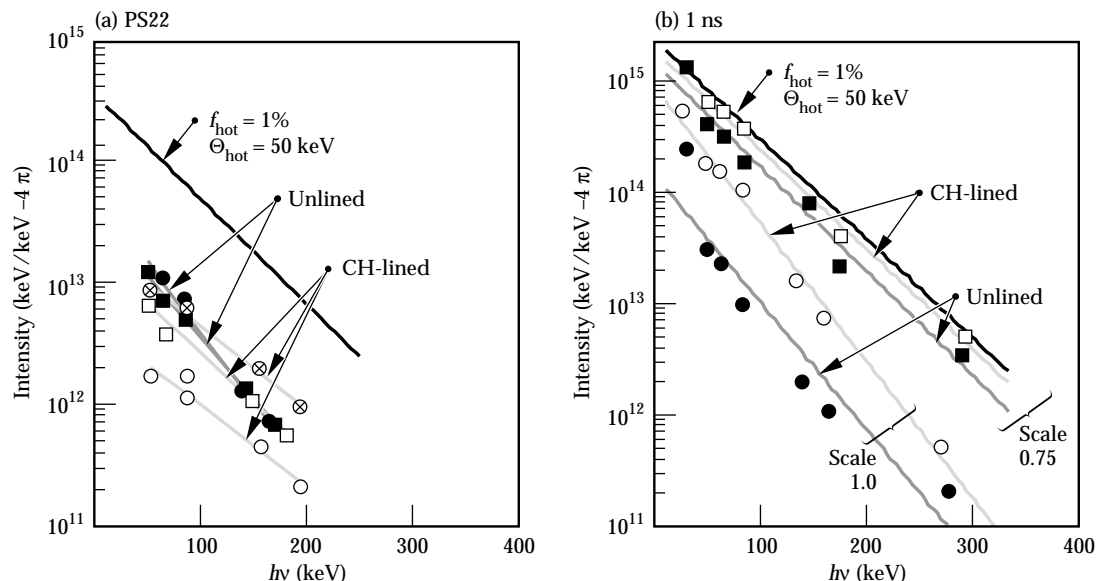
The superthermal electron production is higher for both CH-lined and unlined hohlraums heated with 1-ns pulses at high powers. Figure 8(b) shows experiments using 30-TW pulses. For comparison, the black line denotes a fast-electron fraction of 5% with a 50-keV hot-electron temperature. For the scale-1 hohlraums, fast-electron fractions are 0.4 and 1.8% for unlined and CH-lined hohlraums, respectively. For scale-0.75 hohlraums, the fast-electron fractions are 3% and 3.8%, for unlined and CH-lined hohlraums, respectively. The fast-electron production levels in unlined hohlraums qualitatively agree with levels measured in disk experiments for similar laser irradiances on the hohlraum wall.¹⁷ Irradiances on the hohlraum wall are $\sim 1.3 \times 10^{15}$ W/cm² and $\sim 2.3 \times 10^{15}$ W/cm² for scale-1 and scale-0.75 hohlraums, respectively. Fast-electron production in disk experiments are ~ 1 – 2% with irradiances above 10^{15} W/cm². The higher levels inferred in hohlraums may be due to less loss of fast-electron energy to hydrodynamic expansion and the hohlraum walls absorbing a greater fraction of the electrons. The underdense profiles in hohlraums may also be altered with

increasing scalelengths at, or below, quarter critical density due to plasma confinement, which also could enhance SRS production. Levels for CH-lined hohlraums are slightly above unlined hohlraums but are still only a small part of the overall energy budget. The increase in fast-electron levels may be due to less collisional damping in the low-Z underdense plasma for the CH-lined hohlraums. Simulations, as discussed below, suggest that SRS is produced in the underdense plasma near the transition region between the Au and CH. The observations are consistent with these results. SRS light measurements were not made in these experiments.

Recent experiments using the FABS and NBI indicate that SRS light is highly collimated in the backward direction and that total levels can be much higher than inferred from the scattered light diodes or from hard x-ray bremsstrahlung measurements.⁸ SRS levels of 13% have been observed for one shot in a scale-0.75 unlined hohlraum heated with ~ 25 kJ in a 1-ns square pulse, which is significantly higher than the 3% inferred from x-ray bremsstrahlung. For PS22, SRS levels from FABS and NBI are ~ 2 – 3% compared with $\sim 0.1\%$ levels inferred from x-ray bremsstrahlung. Conversely, SRS levels are $\sim 1\%$ for a scale-1 unlined hohlraum heated with a 1-ns square pulse, which is comparable to levels inferred from x-ray bremsstrahlung. No FABS and NBI data have been taken for lined hohlraums, so the SRS levels scattered into the lens are not known.

Despite the uncertainties in scattered light measurements, lined hohlraums do not show significantly larger scattering losses for most targets compared with unlined hohlraums. For scale-1 targets heated with 1-ns pulses, SBS from CH-lined hohlraums is ~ 2 – 3% comparable to unlined hohlraums, and f_{hot} from CH-lined

FIGURE 8. The x-ray bremsstrahlung spectra from hohlraums heated with (a) PS22 and (b) 1-ns square pulses. The data and fit from unlined (lined) hohlraums are the open (closed) symbols and dark gray (light gray) lines, respectively. The black lines are calculated spectra for f_{hot} of 1% (5%) for PS22 (1-ns square) laser pulse with a T_{hot} of 50 keV. (20-05-1093-3874pb01)



hohlraums is $\sim 2\%$, a factor of two higher than unlined hohlraums. Even correcting for more recent scattering data, the targets still have $f_{\text{abs}} > 90\%$. For scale-0.75 hohlraums with 1-ns pulses, recent measurements from unlined hohlraums show higher levels of f_{SRS} than set by the HLP goals consistent with the lower η_{HOHL} . Beam smoothing techniques have not been applied to lined hohlraums. The lined hohlraums show slightly increased levels of f_{hot} but not enough to explain the decreased drive. For shaped pulses, f_{SBS} is $\sim 15\%$ for Ni-lined hohlraums compared with 5–7% for unlined or CH-lined hohlraums. A 10% reduction in coupling for PS22 would result in about a 5-eV-lower T_{R} consistent with the difference in drive between CH- and Ni-lined hohlraums. Although scattering losses can explain some of the differences in observed coupling, much of the reduction in drive for lined hohlraums is probably due to the difference in energy partition, as discussed in the “LASNEX Modeling” section of this article. All these results are for unsmoothed laser beams. Beam smoothing has been effective in reducing stimulated scattering levels in recent gas-filled hohlraum experiments.^{8,15}

Semi-Empirical Modeling

The power balance model described in Eq. (1) provides a reasonable fit to the data for unlined hohlraums. Although the data set is not as extensive for lined hohlraums, the model also can explain the data, but with a reduced coupling efficiency. The model depends

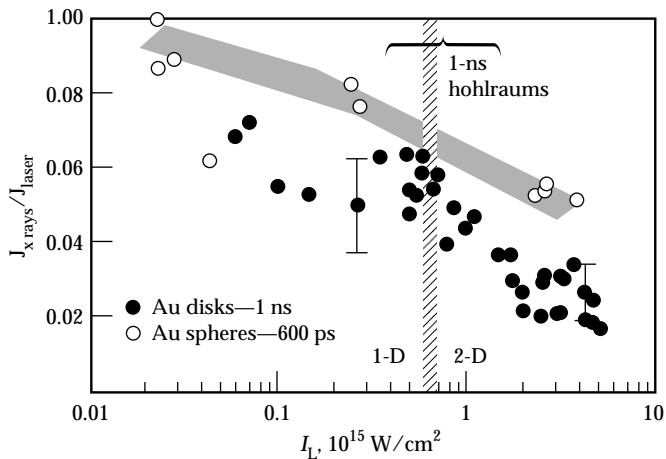


FIGURE 9. Conversion efficiency of converting laser energy into x rays from 0.1–4 keV vs laser intensity I_L . The solid circles are data from single-beam irradiation of Au disks with 1-ns pulses of 0.35- μm light. The open circles are data from Au spheres uniformly irradiated. The bracket denotes the range of intensities on the wall of a scale-1 Nova hohlraum whose data is shown in Fig. 5. The shaded bar shows the division between the regions where the underdense plasma expansion is quasi-1-D vs 2-D. (20-05-1292-3811pb01)

on two parameters: α and η_{HOHL} . The other parameters depend on hohlraum geometry and are usually assumed to be defined by the target geometry although, in principle, they could vary during the experiment due to plasma motion. Parts of NTC tasks are to study the wall albedo and laser coupling efficiency. The wall albedo experiments use burn-through patches measuring the time for the radiation wave to heat a known thickness of Au. These experiments show that present opacity and radiation wave models correctly predict burn-through times for x-ray drive above 200 eV. Details of these experiments have been reported elsewhere.¹⁸

Two sets of experiments have investigated the effective efficiency for converting laser light to drive energy. In one set of experiments defined in HLP7, the conversion efficiency of laser light to x rays using planar disk targets η_{DISK} is studied. The other experiment investigates the difference in x-ray production between disk targets and hohlraums.

Scaling of x-ray conversion efficiency, η_{DISK} , has been studied as a function of laser intensity I_L , using 1-ns square laser pulses of 0.35- μm light. Figure 9 shows the results. The laser energy for most of the shots is ~ 1.5 kJ using a single beam of Nova. Intensity is varied by changing the spot size on the target. The x-ray intensity includes the spectrum from 0.1 to ~ 4 keV. The intensity from 0.1 to 1.5 keV is measured using the XRD array and the intensity in the 2–4 keV range is measured using absolutely calibrated x-ray spectrographs. For disk experiments shown in Fig. 9, η_{DISK} varies from 0.6 to 0.4 for intensities in the range of $\sim 4 \times 10^{14}$ W/cm² to 1.3×10^{15} W/cm². This is the intensity range of the initial wall irradiances for scale-1 hohlraums in Fig. 5 where η_{HOHL} is ~ 0.75 . For scale-0.75 hohlraums, the initial wall irradiance is $\sim 2.3 \times 10^{15}$ W/cm² and η_{HOHL} is ~ 0.65 while η_{DISK} is ~ 0.25 at that intensity. Some of the lower conversion efficiency for a disk may be due to 2-D effects, especially at the higher intensity where the spot size is smaller than the expanding plasma. This transition is noted by the shaded line in Fig. 9 that denotes the estimated transition region between 1-D and 2-D corona expansion. For comparison, conversion efficiency from Au spheres, which are more uniformly irradiated, indicate a higher conversion efficiency (as shown in Fig. 9). Higher efficiencies are also obtained using longer pulses. Instantaneous conversion efficiencies increase from 50% after 1 ns to $\sim 70\%$ at 3 ns for an intensity of $\sim 4 \times 10^{14}$ W/cm².¹⁹

As discussed below, the hydrodynamic losses are reduced in a hohlraum as the hohlraum walls confine the underdense plasma expansion and more energy couples into x-ray heating. To test this modeling, experiments compared the brightness of the laser irradiated spot inside of the hohlraum with the brightness of the spot on a laser-irradiated disk. The results show

that the peak brightness for both the hohlraum and the disk is similar, but the extent of the bright spot in the hohlraum is greater and consistent with the enhanced conversion efficiency in the hohlraum. The increase in size of the hot spot in a hohlraum, as a function of time, is shown in Fig. 10 for a 1-ns square pulse experiment. The increase in width of the emission spot is plotted for three shots as a function of time for emission at 450 eV in Fig. 10(a) and 1200 eV in Fig. 10(b), defined by broadband filters and grazing incident x-ray mirrors.²⁰ The initial width is consistent with the size of the laser beam on the hohlraum wall. The increase in spot size is consistent with LASNEX predictions of the spot width, which are also shown in Fig. 10 (see the shaded circles).

Limited theoretical and experimental work has been done on extending the power balance model to lined hohlraums. The effect of the liner should be minimal on the dynamics of x-ray heating on the wall. The liner thicknesses used are typically optically thin to the radi-

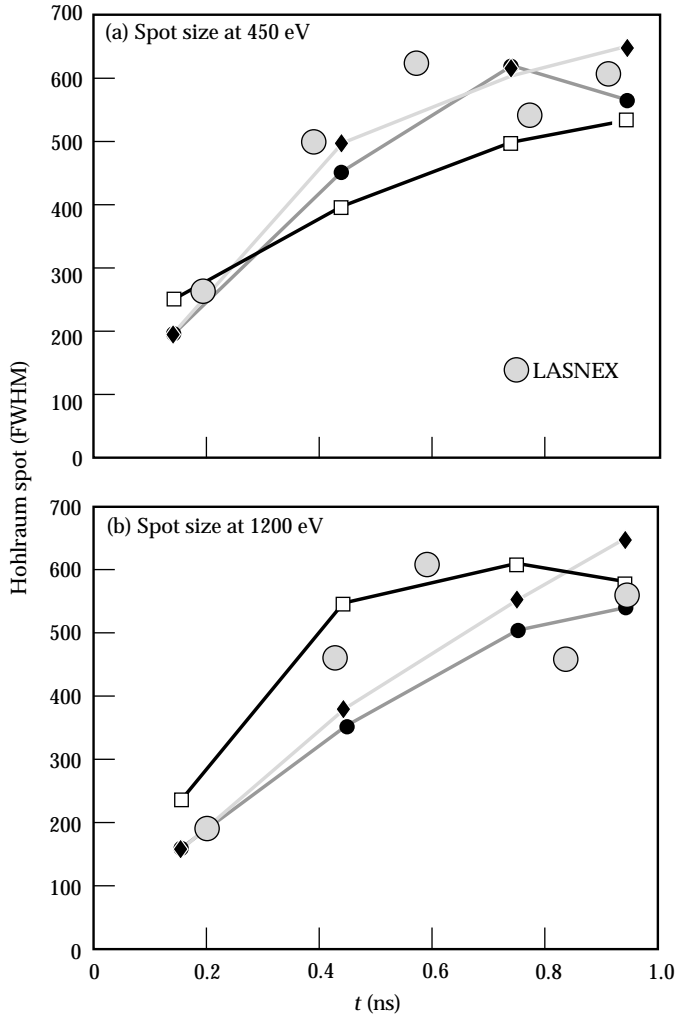


FIGURE 10. The full width at half maximum (FWHM) of the hot spot in a hohlraum produced by the laser spot vs time. The data is taken from three shots for x rays at (a) 450 eV and (b) 1200 eV. (20-05-1292-3806pb01)

ation. Assuming cold opacities,²¹ the 7500-Å CH and 1500-Å Ni liners are ~ 1.5 and 1 Planck mean-free paths thick, respectively, to a 200-eV blackbody radiator. These decrease significantly to much less than one optical depth when the plasma is heated to 100 eV.²² The low- Z plasma therefore should not significantly modify the radiation heating dynamics of the wall (verified by LASNEX calculations).

To test the effects of the thin overcoat on laser hohlraum coupling, x-ray production from Ni-coated Au disks has been measured in a limited number of disk experiments. No experiments have been done on CH-coated disks. Figure 11 compares the conversion efficiency from the overcoated disks with that of pure Au disks as a function of time. Two experiments are done at $\sim 4 \times 10^{14}$ W/cm² with 2-ns square pulses and one experiment is done at $\sim 1 \times 10^{15}$ W/cm² with a 1-ns pulse. The data show a slight delay in x-ray production (~ 200 ps) for a Ni overcoat compared with a Au disk. The time required to burn through the Ni overcoat is estimated to be ~ 100 – 300 ps depending on the model and laser intensity.²³ After the initial burn-through of the Ni, x-ray production is nearly equal to that of Au for 4×10^{14} W/cm² but is only 50% of the pure Au conversion efficiency for 1×10^{15} W/cm². The effect of the overcoat on x-ray production at high intensity is not presently understood. At high intensity the laser spot is smaller than corona expansion scales and is in the 2-D regime. Possible effects of lateral transport and conduction could be affecting the conversion efficiency.

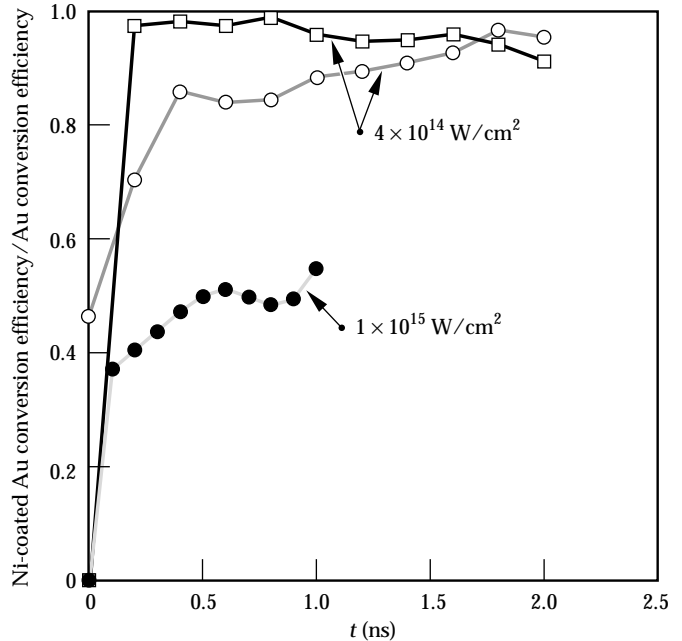


FIGURE 11. The ratio of x-ray conversion efficiency from a 1500-Å Ni coated Au disk to an uncoated Au disk vs time. Data are from a 0.35- μ m laser irradiation of 4×10^{14} W/cm² in a 2-ns square pulse and 1×10^{15} W/cm² in a 1-ns square pulse. (20-05-1095-2365pb01)

LASNEX Modeling

Using LASNEX, extensive work has been done modeling the hohlraums.²⁴ Calculations are fully “integrated” and 2-D. The laser deposition is modeled by using a 2-D representation of the 3-D Nova laser irradiation geometry in a statistical ray generation method. To extract radiation drive from the simulation, a small “virtual” sphere is placed at the center of the hohlraum simulation, and incident flux on the sphere is calculated. The simulations reproduce the x-ray drive measured in unlined hohlraums quite well. Figure 5, shown earlier, compares the peak drive calculated for 1-ns laser pulses with shock velocity measurements. The simulations assume 100% absorption consistent with experiments for scale-1 unlined hohlraums where absorption is greater than 95%. Simulations also reproduce drive in shaped-pulse experiments. LASNEX calculates a peak drive of 215 eV for PS22 when time-dependent SRS and SBS scattering and diagnostic hole losses are included.

Simulations have also been done for several of the lined hohlraum experiments. Generally, the peak drive is calculated to be lower for lined hohlraums compared with unlined hohlraums. Table 1 lists the decrease in calculated peak drive and compares it with experimental decrements. The lower peak drive agrees with the measurements within the statistical uncertainty of the data. The one data set that has the largest difference is the PS22 Ni-lined data. The calculations assume no change in absorption between lined and unlined targets. When the Ni-lined data is reduced by ~10% for the increased f_{SBS} of ~10%, the calculations and data show even better correlation.

Lined hohlraums are calculated to be cooler because more energy couples into plasma blowoff compared with unlined hohlraums. Figure 12 shows calculations

of the energy partitioning in an unlined Au hohlraum and a 2150-Å Ni-lined hohlraum. The energy in wall blowoff, defined as the energy contained in the underdense plasma filling the hohlraum, increases by ~1.5 kJ for the lined hohlraum. This produces a lower T_{R} because it leaves less energy to heat the walls and, self-consistently, to reradiate out the holes. The cause of the increased blowoff energy is due to the higher specific heat for the low-Z blowoff compared with the high-Z blowoff. The specific heat scales

$$\left[\frac{(Z+1)}{A} \right] + E_{\text{ion}}, \quad (2)$$

where Z is the average ion charge and A is the atomic number. For Au irradiated by the laser, Z is ~55 while CH and Ni are nearly fully ionized. The specific heat for Ni and CH are factors of 2 to 2.5 times as high as Au from similar plasma conditions.

Summary

The drive goals for HLP1 and HLP2 are met with over 200 eV obtained for PS22 and 270 eV obtained for a scale-0.75 hohlraum with 30 TW in a 1-ns pulse. The drive is lower for lined hohlraums compared with unlined hohlraums and is generally explained by higher coupling to plasma blowoff in the hohlraums. Although the diagnostics were not optimal for the experiments, the HLP1 coupling goals for f_{abs} , f_{SBS} , f_{hot} , and f_{SRS} appear to have been met for the PS22 CH-lined experiments, although for Ni-lined hohlraums $f_{\text{SBS}} \approx 15\%$. To verify this, more experiments need to be done with the improved Nova diagnostics. The higher levels in Ni-lined hohlraums, compared with CH-lined hohlraums, are consistent with SBS in CH-lined hohlraums being Landau damped by the H and C

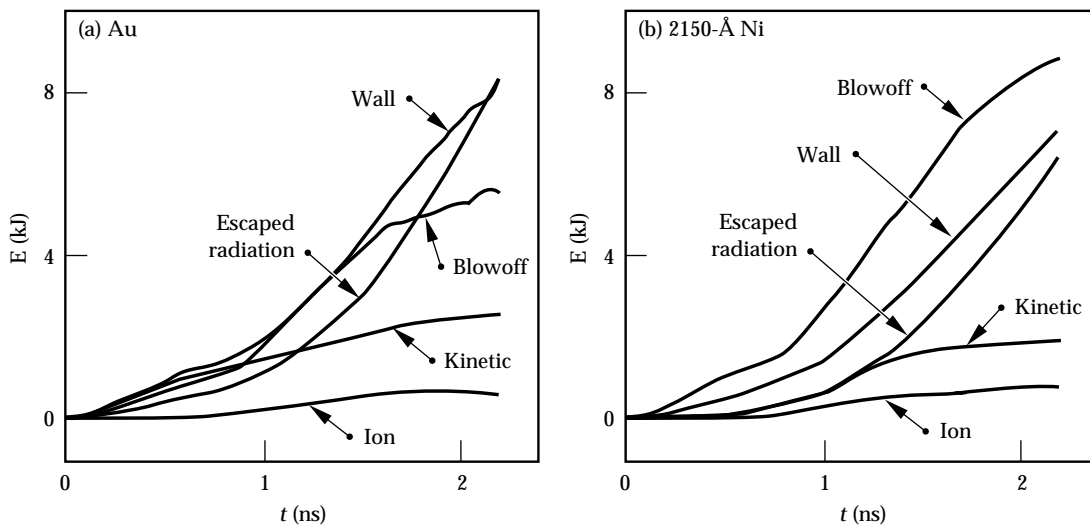


FIGURE 12. Partition of energy E as a function of time from a LASNEX simulation for (a) a pure Au hohlraum and (b) a hohlraum lined with 2150-Å Ni. Both hohlraums are heated with 0.35- μm light using PS22. (50-04-1093-3913pb01)

mixed species plasma.²⁵ By producing a Ni and H mixed liner, Landau damping could also be effective for reducing SBS in the Ni-lined plasmas. For HLP2, the scale-1 hohlraums appear to meet the coupling goals, but f_{SRS} for scale-0.75 hohlraums appear to be higher than 5%. The most recent measurements for unlined scale-0.75 hohlraums is $\sim 13\%$. SRS from lined hohlraums have not been measured, but x-ray bremsstrahlung measurements suggest that f_{SRS} for lined hohlraums may be only slightly higher. The lower η_{HOHL} for scale-0.75 unlined hohlraums is consistent with the measured f_{SRS} and with hohlraum modeling, which includes the scattering models. Future experiments can explore reducing SRS by the use of beam conditioning, as demonstrated in gas-filled hohlraums.¹⁵

Notes and References

1. J. H. Nuckolls, *Phys. Today* 35(9) 24 (1982).
2. J. D. Lindl, *Phys. Plasmas* 2(11), 3933–4024 (1995).
3. L. J. Suter, A. A. Hauer, L. V. Powers, D. B. Rens, et al., *Phys. Rev. Lett.* 73, 2328 (1994).
4. S. W. Haan, S. M. Pollaine, J. D. Lindl, L. J. Suter, et al., *Phys. Plasmas* 2, 2480 (1995).
5. R. L. Kauffman, H. N. Kornblum, D. W. Phillion, C. B. Darrow, et al., *Rev. Sci. Instrum.* 66, 678 (1995).
6. H. N. Kornblum, R. L. Kauffman, and J. A. Smith, *Rev. Sci. Instrum.* 57 2179–81 (1986).
7. P. E. Young, K. G. Estabrook, W. L. Kruer, E. A. Williams, et al., *Phys. Fluids B* 2, 1907–1917 (1990).
8. R. K. Kirkwood C. A. Back, K. S. Bradley, D. H. Kalantar, et al., *Bull. APS* 39, 1753 (1994); B. J. Macgowan et al., “Laser-Plasma Interactions in NIF-Scale Plasmas (HLP5 and HLP6),” p. 305 of this *Quarterly*.
9. *Laser Program Annual Report–1978*, 6–8, Lawrence Livermore National Laboratory, Livermore, CA, UCRL-50021-78 (1979).
10. P. M. Bell, J. D. Kilkenny, G. Power, R. Bonner, and D. K. Bradley, *Ultrahigh Speed and High Speed Photography, Photonics, and Videography '89* (SPIE, Bellingham, WA, 1989; *Proc. SPIE*, 1155) pp. 430–444.
11. R. L. Kauffman, L. J. Suter, C. B. Darrow, J. D. Kilkenny, et al., *Phys. Rev. Lett.* 73, 2320 (1994).
12. R. Sigel, R. Pakula, S. Sakabe, and G. D. Tsakiris, *Phys. Rev. A* 38, 5779 (1988).
13. M. D. Rosen, Lawrence Livermore National Laboratory, Livermore, CA, private communication (1995).
14. R. E. Marshak, *Phys. Fluids* 1, 24 (1958).
15. B. J. MacGowan, R. K. Kirkwood, and D. S. Montgomery, Lawrence Livermore National Laboratory, Livermore, CA, private communication (1995).
16. W. C. Mead, E. M. Campbell, K. G. Estabrook, R. E. Turner, et al., *Phys. Fluids* 26, 2316 (1983).
17. *Laser Program Annual Report–1985*, 4–4, Lawrence Livermore National Laboratory, Livermore, CA, UCRL-50021-85 (1986).
18. J. L. Porter, T. J. Orzechowski, M. D. Rosen, A. R. Thiessen, et al., *1994 ICF Annual Report*, 125, Lawrence Livermore National Laboratory, Livermore, CA, UCRL-LR-105820-94 (1995).
19. F. Ze, D. R. Kania, S. H. Langer, H. Kornblum, et al., *J. Appl. Phys.* 66, 1935–39 (1989).
20. F. Ze, R. L. Kauffman, J. D. Kilkenny, J. Wiedwald, et al., *Rev. Sci. Instrum.* 63, 5124–6 (1992).
21. B. L. Henke, E. M. Gullickson, J. C. Davis, *Atomic Data and Nuclear Data Tables* 54, 181 (1993).
22. *WorkOp–III: 94 Final Report*, Eds., A. Rickert, K. Eidmann, J. Meyer-ter-Vehn, F. J. D. Serduke, and C. A. Iglesias, *Max-Planck-Institut für Quantenoptik* (Report MPQ 204), Hans-Kopferman-Strasse 1, 85748 Garching, Germany (1995).
23. R. Fabbro, C. Max, and E. Fabre, *Phys. Fluids* 28, 1463 (1985).
24. G. B. Zimmerman and W. L. Kruer, *Comments Plasma Phys. Controlled Fusion* 2, 51 (1975).
25. E. A. Williams, R. L. Berger, R. P. Drake, A. M. Rubenchik, et al., *Phys. Plasmas* 2, 129 (1995).